THE ASTROPHYSICAL JOURNAL, 550:793–798, 2001 April 1

OBSERVATIONAL CONSTRAINTS ON THE ABUNDANCE AND EVOLUTION OF "XCN" IN INTERSTELLAR GRAIN MANTLES[1]

D. C. B. WHITTET,[2,3] Y. J. PENDLETON,[4] E. L. GIBB,[2,3] A. C. A. BOOGERT,[5] J. E. CHIAR,[4,6] AND A. NUMMELIN[2,3]
Received 2000 August 3; accepted 2000 November 21

ABSTRACT

The 4.62 μm "XCN" absorption feature, attributed to CN-bearing molecules in solids, is potentially an important diagnostic of the evolution of organic matter in the interstellar medium and the envelopes of newly formed stars. We report quantitative limits on the strength of this feature in the diffuse interstellar medium toward the reddened B-type star Cyg OB2 No. 12 and in the dark cloud toward the young stellar object R CrA IRS 2. On the basis of an assumed band strength for the carrier species, we estimate that less than 0.3% and less than 0.1% of the elemental nitrogen is in CN bonds along these lines of sight, respectively; if they are typical of diffuse and dense environments, it follows that the carrier of XCN is no more than a trace constituent of either organic-refractory or icy interstellar grain mantles. Appreciable XCN abundances seem to occur only in the envelopes of certain young stellar objects (YSOs), most notably the high-mass objects W33A and AFGL 7009S. We confirm the presence of XCN in the spectrum of the low-mass YSO R CrA IRS 7. The strengths of the XCN absorptions in R CrA IRS 7 and other low-mass YSOs indicate mean XCN concentrations relative to H_2O in the ices of $\sim$1%, comparable with the abundance of CN-bearing species in comets.

Subject headings: dust, extinction — infrared: ISM: lines and bands — ISM: molecules

1. INTRODUCTION

The so-called XCN feature, an absorption centered at 4.62 μm in the infrared spectra of certain young stellar objects (YSOs), has been a puzzle since its discovery by Lacy et al. (1984). Although unidentified, the feature is widely attributed to vibrational stretching modes of C$\equiv$N groups in molecular coatings on dust grains. Laboratory experiments suggest that the carrier is formed when interstellar ices containing N-bearing species such as NH_3 or N_2 and C-bearing species such as CH_3OH or CH_4 are subject to irradiation by energetic photons or ions (e.g., Lacy et al. 1984; Bernstein et al. 1995; Pendleton et al. 1999; Palumbo et al. 2000b). If this scenario is broadly correct, the XCN feature has great potential value as a diagnostic of such processing in different environments, from interstellar clouds to protostellar envelopes, where radiation from the embedded star itself may drive chemical evolution. Indeed, processed interstellar ices may constitute an important supply of CN-bearing prebiotic molecules to protoplanetary disks around newly formed stars (e.g., Whittet, Gibb, & Nummelin 2001 and references therein).

The precise nature of the carrier remains elusive. Proposed candidates include nitriles (X$-$C$\equiv$N), isonitriles (X$-$N$\equiv$C), and cyanates (X$-$O$-$C$\equiv$N) (see Pendleton et al. 1999 for a review). However, nitriles appear to be excluded on the basis of poor wavelength agreement: their fundamental C$\equiv$N features occur at 4.4–4.55 μm rather than at 4.62 μm (Bernstein, Sandford, & Allamandola 1997). Although they provide better wavelength coincidence, identification with isonitriles also seems implausible, requiring an uncomfortably low nitrile/isonitrile abundance ratio (<0.1; Gibb et al. 2000a). As isonitriles are intrinsically less stable than the equivalent nitriles (e.g., by 0.63 eV in the case of HNC; Brown 1977), nitrile/isonitrile ratios $\gtrsim 1$ are expected in interstellar clouds—as is, indeed, observed in the gas phase (DeFrees, McLean, & Herbst 1985; Cernicharo et al. 1988; Kawaguchi et al. 1992; Schilke et al. 1992; Hirota et al. 1998). Laboratory experiments involving isotopic substitution techniques provide evidence for a carrier that involves oxygen as well as carbon and nitrogen (Grim & Greenberg 1987; Schutte & Greenberg 1997; Bernstein, Sandford, & Allamandola 2000; Palumbo, Pendleton, & Strazzulla 2000a). Possibilities include cyanate anions (OCN^-; Grim & Greenberg 1987; Schutte & Greenberg 1997; Demyk et al. 1998) or organic residues with $-$O$-$C$\equiv$N attachments (Palumbo et al. 2000b). However, the latest isotopic substitution experiments also implicate hydrogen in the carrier, a result that presents a challenge to the OCN^- hypothesis (Bernstein et al. 2000; Palumbo et al. 2000a).

Emission-line studies of interstellar gas add another twist to the XCN story. Many C$\equiv$N bonded species are known to exist, including nitriles (e.g., HCN, CH_3CN, CH_2CHCN, CH_3CH_2CN) and the cyanopolyynes ($HC_{2n+1}N$). Nitrile abundances are generally low ($<10^{-8}$ with respect to hydrogen) in cold molecular clouds but tend to be enhanced by factors of 10 or more in regions of hot gas near newly formed massive stars (e.g., Blake et al. 1987; Schilke et al. 1992; Liu & Snyder 1999; Gibb et al. 2000b). Gaseous CH_2CHCN and CH_3CH_2CN have been shown to concentrate within a region small compared with the Oort cloud in

[1] Based on observations with *Infrared Space Observatory*, an ESA project with instruments funded by ESA Member States (especially the PI countries: France, Germany, the Netherlands, and the United Kingdom) and with the participation of ISAS and NASA.

[2] Department of Physics, Applied Physics and Astronomy, Rensselaer Polytechnic Institute, Troy, NY 12180; whittd@rpi.edu.

[3] New York Center for Studies on the Origins of Life, Rensselaer Polytechnic Institute, Troy, NY 12180.

[4] NASA Ames Research Center, Mail Stop 245-3, Moffett Field, CA 94035.

[5] Downs Laboratory of Physics, Mail Code 320-47, California Institute of Technology, Pasadena, CA 91125.

[6] SETI Institute, Mountain View, CA 94043.

the envelope of a protostar in the Sgr B2 molecular cloud (Liu & Snyder 1999). Although hot gas-phase chemistry may account for many such species, others may be the product of surface chemistry and ice-mantle evaporation (Charnley, Tielens, & Millar 1992). It is therefore perhaps surprising that there is no evidence for nitriles in interstellar ices. The gas-phase nitrile concentrations in hot cores would require C≡N ice features of optical depth $\tau \sim 1$ near 4.5 μm in the precursor clouds prior to evaporation if all nitriles originated in the ice, whereas the limit toward W33A is a factor of at least 20 below this (Gibb et al. 2000a, 2000b). On the other hand, if XCN is truly a cyanate-bearing species, we should expect high gas-phase cyanate abundances in hot cores. The only such molecule currently identified in the interstellar medium (ISM) is isocyanic acid, HNCO, which appears to be present with an abundance $\sim 10^{-9}$ (e.g., Nummelin et al. 2000; note that the HNCO isomer is more stable than HOCN). HNCO is not itself a candidate for XCN as its CN vibrational mode produces a feature at too short a wavelength ($\sim$4.4 μm), but it may be implicated as a precursor of OCN^- (Schutte & Greenberg 1997).

To better constrain the nature of the XCN carrier, it is important to determine the observational properties of the 4.62 μm infrared feature in lines of sight that sample a wide range of environments. To date, the majority of sources examined in detail for the possible presence of XCN absorption have been high-mass YSOs embedded in molecular clouds, in which any observed feature is assumed to arise in partially processed ices. However, if the carrier resides in an organic residue, detection in other environments may be feasible: such residues are relatively refractory—indeed, solids of this type have been discussed widely as a possible major component of carbonaceous dust in the general ISM (Li & Greenberg 1997) and comets (Briggs et al. 1992). If XCN is a constituent of organic refractory mantles, it should be ubiquitous, with an appreciable abundance in diffuse clouds. If diffuse-cloud grains are recycled into dense clouds, XCN may also be detectable in regions of molecular clouds remote from embedded sources.

The primary aim of this paper is to set a firm quantitative limit on the abundance of XCN in the "diffuse ISM"—taken here to mean regions of relatively low density ($n \lesssim 100$ cm^{-3}) where hydrogen is predominantly atomic rather than molecular and dust grains lack icy mantles. Background sources traditionally used to sample this phase of the ISM include the Galactic center infrared sources (Chiar et al. 2000 and references therein) and a small number of highly reddened, luminous stars, most notably the B-type hypergiant Cyg OB2 No. 12. The Galactic center has the advantage of relatively high extinction ($A_V \sim 30$ mag), but unfortunately the 4.4–4.8 μm region containing the XCN feature is heavily contaminated with strong gas-phase CO absorption lines. Also, a significant fraction of the total extinction toward the Galactic center is now known to arise in molecular clouds (Whittet et al. 1997; Chiar et al. 2000). We select Cyg OB2 No. 12 as the target best suited to our objective.

Other environments of interest include quiescent dark clouds and low-mass YSOs: only a few such sight lines have been examined previously (Tegler et al. 1993, 1995; Weintraub et al. 1994). We present new constraints on the XCN abundance in three low-mass YSOs in the R CrA dark cloud, a region known (from the high abundance of solid CO in the ices; see Chiar et al. 1998) to be relatively quiescent. Such objects are potentially important as they may represent reasonable analogs of the early solar system.

2. OBSERVATIONS AND RESULTS

2.1. *Cygnus OB2 No. 12*

Cyg OB2 No. 12 is located at a distance of $\sim$1.7 kpc, behind some 10.2 mag of visual extinction arising in diffuse-cloud dust along the line of sight (see Whittet et al. 1997 for a brief review). The observations used here were obtained with the Short-Wavelength Spectrometer (SWS) of the *Infrared Space Observatory* (*ISO*) (de Graauw et al. 1996). Cyg OB2 No. 12 was observed in full grating scan mode (template S01, speed 3) on two occasions (1996 April 4 and 1996 October 17). In each case, the total integration time was $\sim$3450 s and the mean spectral resolving power was $\lambda/\Delta\lambda \sim 400$ over the full 2.4–45 μm spectral range of the SWS. Both spectra were reduced using the standard SWS Interactive Analysis package (de Graauw et al. 1996). The 1996 October spectrum was published previously by Whittet et al. (1997), but the data have been re-reduced using a more recent version of the pipeline process (OLP7.01) with improved calibration files.[7] The 1996 April spectrum was obtained from the *ISO* data archive and reduced in exactly the same way.

Figure 1 shows the two spectra in the wavelength range 2.4–7.8 μm. To convert each flux spectrum into optical depth, a fourth-order polynomial fitted to selected wavelength ranges was used to represent the continuum. The regions chosen were 2.4–2.5, 2.7–2.74, 2.9–3.0, 3.2–3.25,

[7] An apparent shallow feature near 2.7 μm in the 1996 October spectrum of Cyg OB2 No. 12, tentatively attributed to hydrated silicates (Whittet et al. 1997), is not convincingly present in the re-reduced spectrum; it appears to have been an artifact of the calibration file then in use. The past trend has been for apparent shallow features to disappear as the calibration has been refined. It seems very unlikely that any future refinements will affect the results of the present paper (e.g., by introducing a feature not evident at present in the XCN wavelength).

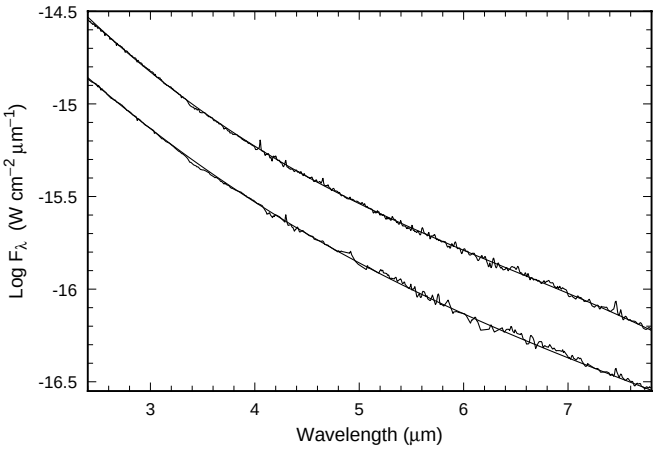

FIG. 1.—Two 2.4–7.8 μm SWS spectra of Cyg OB2 No. 12, together with the adopted continuum fits (*smooth curves*) described in § 2.1. The flux scale refers to the upper spectrum (1996 October 17 data); the lower spectrum (1996 April 4 data) has been displaced downward by 0.3 dex in log F_λ for display.

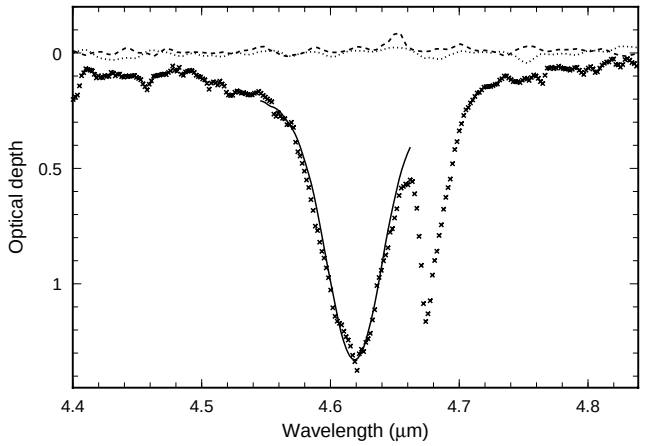

FIG. 2.—Comparison of optical depth spectra in the region of the 4.62 μm XCN feature for Cyg OB2 No. 12, W33A, and a laboratory residue. *Dotted and dashed curves:* SWS spectra of Cyg OB2 No. 12 from 1996 April 4 and 1996 October 17, respectively. *Points:* SWS spectrum of W33A from Gibb et al. (2000a). *Solid curve:* Spectrum of a laboratory residue produced by ion bombardment of an ice mixture containing $H_2O:N_2:CH_4 = 1:1:1$ (Palumbo et al. 2000b), scaled to match the feature in W33A. Note that the W33A spectrum contains a very broad, weak absorption feature (the combination mode of H_2O ice, centered at $\sim$4.5 μm with peak optical depth $\sim$0.1; Gibb et al. 2000a) that overlaps this entire spectral region, as well as a narrow, deep feature near 4.675 μm attributed to solid CO.

3.86–4.0, 4.95–5.1, 5.5–5.6, and 7.7–7.8 μm. These were selected to give a reasonable distribution across the spectrum while avoiding known interstellar features (e.g., hydrocarbons at 3.4 μm; silicates at 8–12 μm) and major photospheric/chromospheric lines (e.g., hydrogen Brα and Pfα emission at 4.05 and 7.46 μm, respectively[8]). The resulting fits are shown in Figure 1.

Optical depth spectra covering the range 4.4–4.8 μm in Cyg OB2 No. 12 are shown in Figures 2 and 3. Also shown for comparison in Figure 2 are data for W33A (the source

[8] Cyg OB2 No. 12 appears to have undergone intrinsic spectral variability in the time interval between the two sets of observations, with H emission lines more prominent in the later spectrum.

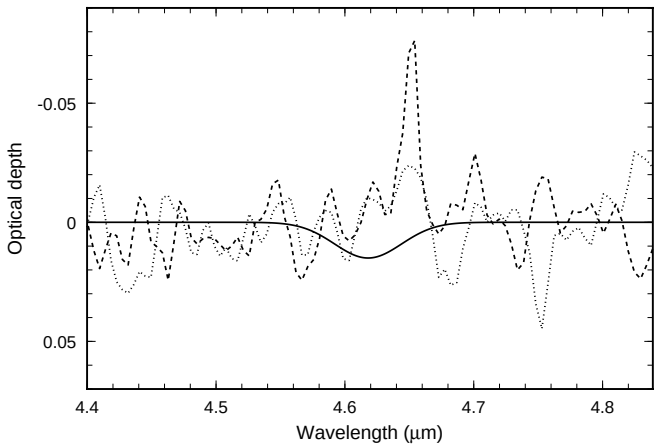

FIG. 3.—Enlargement of optical depth spectra in the region of the 4.62 μm XCN feature for Cyg OB2 No. 12. Dotted and dashed curves are the same as in Fig. 2. The peak at 4.654 μm (most prominent in the 1996 October 17 spectrum) is identified with stellar Pfβ line emission. The solid curve is a Gaussian profile (eq. [1]) representing our estimated upper limit on the strength of the putative XCN feature. The parameters of the profile are $\lambda_0 = 4.618$ μm, $\sigma = 0.026$ μm, and $\tau_{max} = 0.015$.

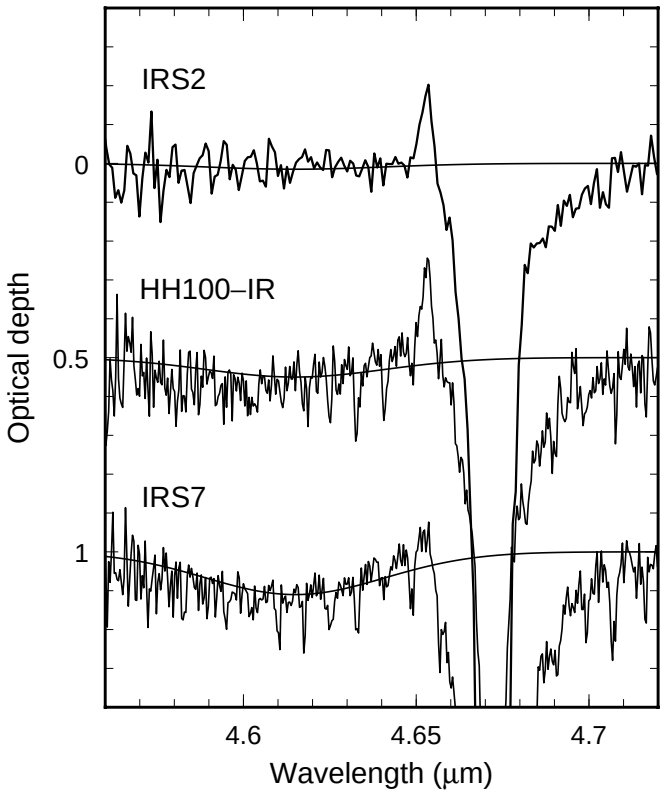

FIG. 4.—Optical depth spectra in the region of the 4.62 μm XCN feature for three R CrA sources, based on data from Chiar et al. (1998). The vertical scale refers to the IRS 2 spectrum; the HH 100–IR and IRS 7 spectra have been displaced downward by 0.5 and 1.0 optical depth units, respectively, for display. Peaks at 4.654 μm correspond to the Pfβ line, and the deep trough at 4.66–4.69 μm is attributed to interstellar solid CO absorption. Narrow absorption lines of gas-phase CO are also evident in the spectra of HH 100-IR and IRS 7. Solid curves are Gaussian profiles (eq. [1]) representing XCN, scaled to match the observed spectra. Parameters of the profiles are $\lambda_0 = 4.615$ μm and $\sigma = 0.019$ μm, with $\tau_{max} = 0.015$ (IRS 2), 0.05 (HH 100–IR), and 0.11 (IRS 7).

with the deepest known XCN feature) and a laboratory residue. It is evident that no appreciable absorption feature is present at 4.62 μm in Cyg OB2 No. 12. To evaluate a limit on the strength of the feature, the Cyg OB2 No. 12 spectra are compared in Figure 3 with a Gaussian profile,

$$\tau(\lambda) = \tau_{max} \exp\left\{\frac{-(\lambda - \lambda_0)^2}{2\,\sigma^2}\right\}, \quad (1)$$

where $\lambda_0 = 4.618$ μm and $\sigma = 0.026$ μm (FWHM = 2.35 $\sigma = 0.061$ μm), which provides a fair representation of the XCN profile in both W33A and the laboratory residue (Fig. 2). Stellar Pfβ emission at 4.65–4.66 μm overlaps the long-wavelength wing of XCN, but the 4.58–4.64 μm region should be free of contamination. A range of possible values of τ_{max} was considered (eq. [1]); the curve shown in Figure 3 has $\tau_{max} = 0.015$, which we take as the upper limit.

2.2. *Infrared Sources in the R CrA Dark Cloud*

Ground-based 4.55–4.75 μm spectra of three infrared sources associated with low-mass YSOs in the R CrA dark cloud were previously reported by Chiar et al. (1998). The sources are R CrA IRS 1, IRS 2, and IRS 7 (IRS 1 is also known as HH 100–IR, and we adopt the latter designation here; see Whittet et al. 1996 for a review of this line of sight). Chiar et al. (1998) carried out a detailed analysis of solid CO

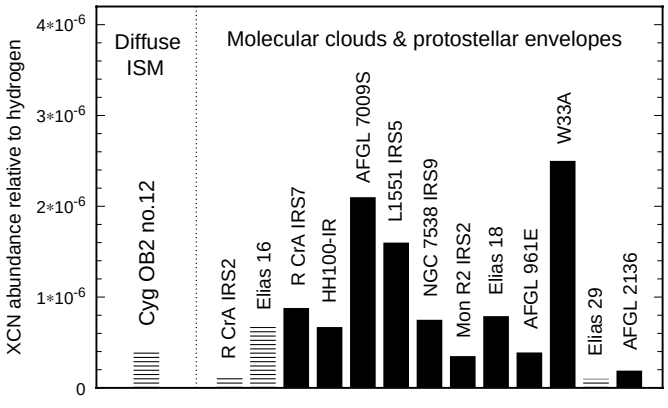

FIG. 5.—Bar chart of XCN abundance relative to total hydrogen column density (Table 1) with respect to environment. Hatched bars denote upper limits. Sources that sample molecular clouds and/or protostellar envelopes are sequenced from left to right in order of descending solid CO abundance relative to total hydrogen.

features in these sources and noted the presence of 4.62 μm XCN absorption in IRS 7. Here, we present quantitative measurements and limits on XCN.

The spectra (Fig. 4) were obtained in 1995 May (IRS 2) and 1996 April (HH 100–IR and IRS 7) with the grating spectrometer CGS4 on the United Kingdom Infrared Telescope at Mauna Kea Observatory in Hawaii. The spectral resolving power is $\lambda/\Delta\lambda \sim 1800$. Full details of the observations and data reductions may be found in Chiar et al. (1998). The 4.654 μm H Pfβ line is seen in emission in HH 100–IR and IRS 2 and is probably also weakly present in IRS 7. Narrow absorption lines arising in the P and R branches of gas-phase CO are evident in the spectra of HH 100–IR and IRS 7. In the case of IRS 2, CO appears to be predominantly in the solid phase, resulting in a very deep 4.675 μm feature (Chiar et al. 1998). Broad, shallow 4.58–4.65 μm absorption corresponding to the XCN feature is clearly present in IRS 7 and can be excluded in IRS 2; in the case of HH 100–IR, the data are consistent with a weak XCN feature (although peak absorption appears to be centered at 4.60 rather than 4.62 μm). Profiles (eq. [1]) were fitted by eye to the spectra, ignoring data points affected by Pfβ emission and CO absorption lines. Results are shown in Figure 4 (*smooth curves*). The curve for IRS 2 represents an upper limit of $\tau_{max} < 0.015$, that for HH 100–IR a tentative detection with $\tau_{max} = 0.05 \pm 0.03$; for IRS 7 we deduce $\tau_{max} = 0.11 \pm 0.015$.

3. ABUNDANCES

The column density of C≡N groups that contribute to the 4.62 μm feature in a given line of sight is related to its strength by

$$N = \frac{\int \tau_\nu \, d\nu}{A}, \tag{2}$$

where ν is the wavenumber, A is the band strength of the feature in cm molecule^{-1}, and the integration is carried out over the entire profile. As the observed profile (e.g., W33A, Fig. 2) appears to be smooth and symmetrical, N may be estimated to a good approximation from

$$N \approx \frac{\tau_{max} \Delta\nu}{A}, \tag{3}$$

where $\Delta\nu$ is the FWHM of the XCN feature. The value of A appropriate to the carrier of the interstellar feature is constrained by laboratory measurements for candidate

TABLE 1

CATALOG OF XCN AND CO ABUNDANCES

Line of Sight	N(XCN)[a] (10^{17} cm^{-2})	N(CO)[b] (10^{17} cm^{-2})	N(H)[c] (10^{22} cm^{-2})	$\frac{N(\text{XCN})}{N(\text{H})}$	$\frac{N(\text{CO})}{N(\text{H})}$	References
Diffuse Interstellar Medium						
Cyg OB2 No. 12	<0.084	...	2.0	$<4.2 \times 10^{-7}$	...	1, 2
Molecular Clouds and Protostellar Envelopes						
R CrA IRS 2	<0.084	12	7.0	$<1.2 \times 10^{-7}$	1.7×10^{-5}	1, 3
Elias 16 (Taurus)	<0.28	6.5	4.2	$<6.7 \times 10^{-7}$	1.5×10^{-5}	4, 5
R CrA IRS 7	0.62	10	7.0	8.8×10^{-7}	1.4×10^{-5}	1, 3
HH 100–IR	0.34	6.5	5.0	6.7×10^{-7}	1.3×10^{-5}	1, 3, 6
AFGL 7009S	4.2	18	20	2.1×10^{-6}	9.0×10^{-6}	7, 8, 9
L1551 IRS 5	0.64	3.2	4.0	1.7×10^{-6}	8.0×10^{-6}	10
NGC 7538 IRS 9.....	1.2	12	16	7.5×10^{-7}	7.5×10^{-6}	11, 3
Mon R2 IRS 2	0.14	2.7	4.0	3.5×10^{-7}	6.8×10^{-6}	11, 3
Elias 18 (Taurus)	0.28	2.3	3.5	7.9×10^{-7}	6.6×10^{-6}	4, 5
AFGL 961E	0.29	2.9	7.4	3.9×10^{-7}	3.9×10^{-6}	11, 3, 12
W33A.....	6.9	8.9	28	2.5×10^{-6}	3.2×10^{-6}	13, 3, 12
Elias 29 (ρ Oph).....	<0.06	1.7	12	$<4.7 \times 10^{-8}$	1.4×10^{-6}	14
AFGL 2136.....	0.34	1.1	18	1.9×10^{-7}	6.1×10^{-7}	11, 12

[a] Solid-state column density, calculated from eq. (3) with $A = 5 \times 10^{-17}$ cm molecule^{-1}; $\Delta\nu = 28$ cm^{-1} is assumed in cases where no measured value is quoted in the literature.

[b] Literature values of solid-state CO column density.

[c] Total gas-phase hydrogen column density, estimated from total visual extinction or silicate optical depth, assuming standard conversion factors (e.g., Whittet 1992); see cited references.

REFERENCES.—(1) This paper; (2) Whittet et al. 1997; (3) Chiar et al. 1998; (4) Tegler et al. 1995; (5) Chiar et al. 1995; (6) Whittet et al. 1996; (7) Demyk et al. 1998; (8) d'Hendecourt et al. 1998; (9) Demyk et al. 1999; (10) Tegler et al. 1993; (11) Pendleton et al. 1999; (12) Tielens et al. 1991; (13) Gibb et al. 2000a—note that the XCN band strength assumed here is different from that assumed by Gibb et al. 2000a; (14) Boogert et al. 2000b.

materials. A review of the literature indicates values (in units of 10^{-17} cm molecule^{-1}) of 1–3 for isonitriles in H_2O-ice matrices (Bernstein et al. 1997), 2–4 for photolyzed interstellar ice analogs (d'Hendecourt et al. 1986), and 4–10 for OCN^- (Schettino & Hisatsune 1970; Demyk et al. 1998; W. A. Schutte 2000, private communication). Unfortunately, no measurements of A are available for the organic refractory residues discussed by Palumbo et al. (2000a, 2000b). Somewhat arbitrarily, we adopt a value (5×10^{-17} cm molecule^{-1}) that lies close to the middle of this overall range. Thus, uncertainties in absolute abundances arising from uncertainties in A may be as high as a factor of 2. Comparisons of relative abundances in different regions should not be affected by this source of error provided A does not change systematically with environment.

Solid XCN column densities and abundances are listed in Table 1 and illustrated schematically in Figure 5. Results for Cyg OB2 No. 12 (§ 2.1) and the R CrA objects (§ 2.2) are compared with data available from previous literature. Also given in Table 1 are abundance data for solid CO: As the most volatile ice species commonly observed in grain mantles, its abundance provides a good measure of the average (thermal) evolutionary state of the ices along each line of sight. Note that 12 of the 13 sources in the "molecular clouds and protostellar envelopes" section of the data base are YSOs, the exception being the field star Elias 16, which samples cold molecular material in the Taurus dark cloud (e.g., Whittet et al. 1998). The similarity in solid CO abundance, comparing Elias 16 and the three R CrA sources, suggests that most of the material toward the latter resides in the molecular cloud rather than in protostellar envelopes. The total (gas + solid) CO abundance in molecular clouds is typically $\sim 5 \times 10^{-5}$; hence, the solid phase represents a substantial fraction (20%–50%) of all the CO toward the R CrA sources and Elias 16 (Chiar et al. 1995, 1998) but only a minor fraction ($\lesssim 5\%$) toward YSOs such as W33A and Elias 29, where much of the CO has sublimed (Mitchell, Allen, & Maillard 1988; Boogert et al. 2000b).

With the exception of Cyg OB2 No. 12 (which has no solid CO detection; Whittet et al. 1997), the sources are sequenced in Figure 5 and Table 1 in order of descending solid CO abundance. The expected contribution of cold, quiescent molecular-cloud material to the total dust column along the line of sight thus decreases sequentially from left to right in Figure 5 while the envelope contribution presumably increases correspondingly. The solid CO abundance is thus to some degree a measure of evolutionary state, although it should be used with caution. While a high value seems likely to be a reliable signature of cold molecular clouds, a low value does not necessarily imply that all the ices along a given line of sight are highly thermally processed (see, e.g., the discussion of Elias 29 in Boogert et al. 2000b).

4. DISCUSSION

Our upper limit on the 4.62 μm feature in the spectrum of Cyg OB2 No. 12 shows that interstellar grains in the diffuse ISM along this line of sight are not rich in C≡N–bearing organic molecules. From our result, we estimate that less than 0.3% of the available elemental nitrogen (assuming solar abundance) is in C≡N groups toward Cyg OB2 No. 12. Furthermore, our result for R CrA IRS 2 implies an even tighter limit (<0.1% nitrogen in C≡N) in this dark cloud: Neither icy nor refractory components of the dust toward this object can contain appreciable XCN. For comparison, the XCN/N ratio is ~2% toward the "XCN-rich" objects W33A and AFGL 7009S and ~1% toward lower mass objects such as R CrA IRS 7 and Elias 18. If Cyg OB2 No. 12 and R CrA IRS 2 are typical lines of sight, CN-bearing solids are no more than trace constituents of dust remote from young stars. We conclude that XCN formed in the envelopes of protostars is not returned to the ISM as a major component of refractory dust. Either it does not remain on the dust outside of dense environments, or the injection rate is too small to influence the net composition. This conclusion is consistent with independent evidence demonstrating that the depletion of N into dust in diffuse interstellar clouds is low and insensitive to physical conditions (Meyer, Cardelli, & Sofia 1997).

Several recent studies have demonstrated the significance of thermal processing in the evolution of protostellar ices, especially for high-mass stars (Chiar et al. 1998; Gerakines et al. 1999; Boogert et al. 2000a). This evidence, together with the apparent lack of XCN in general interstellar dust, may be taken as indirect support for the proposal that evaporation of icy mantles is an important route to gas-phase molecules in hot cores. However, as discussed in § 1, there is apparent inconsistency between the evidence from infrared spectroscopy, which favors cyanates as the dominant CN-bearing form in the sublimates, and from millimeter-wave spectroscopy, which indicates systematically enhanced nitrile abundances in hot gas. It is not yet known whether HNCO is similarly enhanced or whether other OCN-bearing species are present in the gas in hot cores. Future observations are needed to address this question. Gas-phase reactions involving species evaporated from grains as reactants may be the primary source of nitriles in hot cores, although it does not seem possible to synthesize ethyl cyanide (CH_3CH_2CN) in this way (Charnley et al. 1992).

CN-bearing species formed in the envelopes of young stars may be incorporated into planetesimals in protoplanetary disks by direct accretion of processed ice mantles or by adsorption of molecules synthesized in the gas. An interesting development is the increasing number of relatively low-mass YSOs known to exhibit appreciable XCN features. The list now includes R CrA IRS 7 and (tentatively) HH 100–IR, as well as Elias 18, L1551 IRS 5, and RNO 91 (Tegler et al. 1993, 1995; Weintraub et al. 1994).[9] The precise nature of the underlying young stars responsible for these infrared sources is not well known, but their masses most likely lie in the 1–5 $M_\odot$ range. It seems safe to conclude that energetic processing needed to drive XCN formation is not the sole prerogative of massive ($\gtrsim 10\ M_\odot$) YSOs such as W33A and AFGL 7009S. However, not all low-mass YSOs show XCN absorption. R CrA IRS 2 and Elias 29 have upper limits well below detection levels in other sources (other nondetections include HL Tau and Z CMa; Tegler et al. 1995). Note that R CrA IRS 2 and Elias 29 lie at opposite extremes of the range in solid CO abundance (Fig. 5). It is therefore tempting to associate XCN production with an intermediate evolutionary phase; however, its presence and detectability may also depend on a number of other factors, such as the mass and morphology of the cir-

[9] Note that RNO 91 was not included in our database (Table 1; Fig. 5) because the hydrogen column density is unknown.

cumstellar disk and the viewing geometry. In the case of Elias 29, separate regions containing hot gas and unprocessed ices appear to be present in the line of sight (Boogert et al. 2000b).

The mean concentration of XCN relative to H_2O in the ices may be estimated using observations of the 3.1 μm H_2O-ice absorption feature. Results for the low-mass YSOs HH 100–IR, R CrA IRS 7, Elias 18, and L1551 IRS 5 (Whittet et al. 1996; Chiar et al. 1998; Tegler et al. 1993) indicate XCN concentrations $\sim$1%–2%. This is presumably a lower limit on the concentration in regions close to each star, as the line-of-sight average is diluted by foreground molecular-cloud material that does not contain XCN. The highest observed XCN concentration is $\sim$6% toward W33A (based on H_2O-ice data from Gibb et al. 2000a). For comparison, the aggregate concentration relative to H_2O of all known C$\equiv$N-bonded molecules in comet C/1995 O1 (Hale-Bopp) is $\sim$0.43% (see Bockelée-Morvan et al. 2000, who argue that this comet is rich in interstellar ices). Species present in Hale-Bopp include HCN, HNC, CH_3CN, HC_3N, and HNCO, of which the latter (the only cyanate detected to date) contributes $\sim$0.1%. HNCO was also detected with similar abundance in comet C/1996 B2 (Hyakutake) (Lis et al. 1997). We conclude that the XCN concentrations in ices surrounding low-mass YSOs seem adequate to explain cometary HNCO abundances if these species are intimately linked.

What do the results of this paper imply for the identity of XCN? We note that the various laboratory analogs discussed in the literature have different volatilities. Grim & Greenberg (1987) attribute XCN to OCN^- anions generated by UV photolysis of ices containing H_2O, NH_3, and CO. They show that the 4.62 μm feature decreases systematically in strength upon subsequent warm-up of the irradiated sample above 140 K and disappears at room temperature. In contrast, the XCN candidate produced in the ion-bombardment experiments of Palumbo et al. (2000b) is stable at room temperature, leading these authors to describe it as "a refractory species well bonded to the residue which also formed as a result of the irradiation." Our results are clearly more consistent with a carrier that remains volatile. If organic refractory residues containing XCN are ubiquitous products of ion bombardment, then UV photolysis is favored as the energy source. In this case, the nature of the nitrogen in the initial ice mixture is also constrained (Elsila, Allamandola, & Sandford 1997; Palumbo et al. 2000b). Whereas XCN-like absorbers are formed by ion bombardment of mixtures containing either NH_3 or N_2, UV photolysis gives a significant yield only with NH_3 as the primary nitrogen carrier.

D. C. B. W. is funded by NASA through JPL contract no. 961624 (*ISO* data analysis) and by the NASA Exobiology and Long-Term Space Astrophysics programs (grants NAG 5-7598, NAG 5-7884, and NAG 5-9148). Y. J. P. is supported by the NASA Exobiology program under grant 344-38-12-09. J. E. C. is supported by the NASA Long-Term Space Astrophysics program under grant 399-20-61-02. We thank an anonymous referee for helpful comments that led to several improvements in this paper.

REFERENCES

Bernstein, M. P., Sandford, S. A., & Allamandola, L. J. 1997, ApJ, 476, 932
———. 2000, ApJ, 542, 894
Bernstein, M. P., Sandford, S. A., Allamandola, L. J., Chang, S., & Scharberg, M. A. 1995, ApJ, 454, 327
Blake, G. A., Sutton, E. C., Masson, C. R., & Phillips, T. G. 1987, ApJ, 315, 621
Bockelée-Morvan, D., et al. 2000, A&A, 353, 1101
Boogert, A. C. A., et al. 2000a, A&A, 353, 349
———. 2000b, A&A, 360, 683
Briggs, R., et al. 1992, Origins Life Evol. Biosphere, 22, 287
Brown, R. D. 1977, Nature, 270, 39
Cernicharo, J., Kahane, C., Guelin, M., & Gomez-Gonzalez, J. 1988, A&A, 189, L1
Charnley, S. B., Tielens, A. G. G. M., & Millar, T. J. 1992, ApJ, 399, L71
Chiar, J. E., Adamson, A. J., Kerr, T. H., & Whittet, D. C. B. 1995, ApJ, 455, 234
Chiar, J. E., Gerakines, P. A., Whittet, D. C. B., Pendleton, Y. J., Tielens, A. G. G. M., & Adamson, A. J. 1998, ApJ, 498, 716
Chiar, J. E., et al. 2000, ApJ, 537, 749
DeFrees, D. J., McLean, A. D., & Herbst, E. 1985, ApJ, 293, 236
de Graauw, Th., et al. 1996, A&A, 315, L49
Demyk, K., Dartois, E., d'Hendecourt, L., Jourdain de Muizon, M., Heras, A. M., & Breitfellner, M. 1998, A&A, 339, 553
Demyk, K., Jones, A. P., Dartois, E., Cox, P., & d'Hendecourt, L. 1999, A&A, 349, 267
d'Hendecourt, L. B., Allamandola, L. J., Grim, R. J. A., & Greenberg, J. M. 1986, A&A, 158, 119
d'Hendecourt, L., Jourdain de Muizon, M., Dartois, E., Demyk, K., Ehrenfreund, P., & Heras, A. 1998, in Proc. ESA Conf., The Universe as Seen by *ISO*, ed. P. Cox & M. F. Kessler (ESA SP-427), 437
Elsila, J., Allamandola, L. J., & Sandford, S. A. 1997, ApJ, 479, 818
Gerakines, P. A., et al. 1999, ApJ, 522, 357
Gibb, E. L., et al. 2000a, ApJ, 536, 347
Gibb, E. L., Nummelin, A., Irvine, W. M., Whittet, D. C. B., & Bergman, P. 2000b, ApJ, 545, 309
Grim, R. J. A., & Greenberg, J. M. 1987, ApJ, 321, L91
Hirota, T., Yamamoto, S., Mikami, H., & Ohishi, M. 1998, ApJ, 503, 717
Kawaguchi, K., Ohishi, M., Ishikawa, S., & Kaifu, N. 1992, ApJ, 386, L51
Lacy, J. H., et al. 1984, ApJ, 276, 533
Li, A., & Greenberg, J. M. 1997, A&A, 323, 566
Lis, D. C., et al. 1997, Icarus, 130, 355
Liu, S.-Y., & Snyder, L. E. 1999, ApJ, 523, 683
Meyer, D. M., Cardelli, J. A., & Sofia, U. J. 1997, ApJ, 490, L103
Mitchell, G. F., Allen, M., & Maillard, J.-P. 1988, ApJ, 333, L55
Nummelin, A., et al. 2000, ApJS, 128, 213
Palumbo, M. E., Pendleton, Y. J., & Strazzulla, G. 2000a, ApJ, 542, 890
Palumbo, M. E., Strazzulla, G., Pendleton, Y. J., & Tielens, A. G. G. M. 2000b, ApJ, 534, 801
Pendleton, Y. J., Tielens, A. G. G. M., Tokunaga, A. T., & Bernstein, M. P. 1999, ApJ, 513, 294
Schettino, V., & Hisatsune, I. C. 1970, J. Chem. Phys., 52, 9
Schilke, P., Walmsley, C. M., Pineau des Forets, G., Roueff, E., Flower, D. R., & Guilloteau, S. 1992, A&A, 256, 595
Schutte, W. A., & Greenberg, J. M. 1997, A&A, 317, L43
Tegler, S. C., Weintraub, D. A., Allamandola, L. J., Sandford, S. A., Rettig, T. W., & Campins, H. 1993, ApJ, 411, 260
Tegler, S. C., Weintraub, D. A., Rettig, T. W., Pendleton, Y. J., Whittet, D. C. B., & Kulesa, C. A. 1995, ApJ, 439, 279
Tielens, A. G. G. M., Tokunaga, A. T., Geballe, T. R., & Baas, F. 1991, ApJ, 381, 181
Weintraub, D. A., Tegler, S. C., Kastner, J. H., & Rettig, T. W. 1994, ApJ, 423, 674
Whittet, D. C. B. 1992, Dust in the Galactic Environment (Bristol: Institute of Physics)
Whittet, D. C. B., et al. 1996, ApJ, 458, 363
———. 1997, ApJ, 490, 729
———. 1998, ApJ, 498, L159
Whittet, D. C. B., Gibb, E. L., & Nummelin, A. 2001, Origins Life Evol. Biosphere, in press